# Fourier-transform MS and Closed-path Multi-reflection Time-of-Flight MS using an Electrostatic Linear Ion Trap

Eric T. Dziekonski, Joshua T. Johnson, Kenneth W. Lee, and Scott A. McLuckey\*

Department of Chemistry
Purdue University
West Lafayette, Indiana, USA 47907-2084

\*Address reprint requests to: Dr. Scott A. McLuckey

560 Oval Drive

Department of Chemistry

Purdue University West Lafayette, IN 47907-2084, USA

Phone: (765) 494-5270

Fax: (765) 494-0239

E-mail: mcluckey@purdue.edu

#### **Abstract**

An electrostatic linear ion trap (ELIT) has been configured to allow for the simultaneous acquisition of mass spectra via Fourier transform (FT) techniques (frequency measurement) and via time-of-flight (TOF) (time measurement). In the former case, the time-domain image charge derived from a pick-up electrode in the field-free region of the ELIT is converted to frequencydomain data via Fourier transformation (i.e., FT-ELIT MS). In the latter case, the time difference between ion injection into the ELIT and ion detection after release from the ELIT using a microchannel plate (MCP) enables the acquisition of multi-reflection time-of-flight mass spectra (MR-TOF MS). The ELIT geometry facilitates the acquisition of both types of data simultaneously because the detection schemes are independent and do not preclude one another. The two MS approaches exhibit a degree of complementarity. Resolution increases much faster with time with the MR-TOF approach, for example, but the closed-path nature of executing MR-TOF in an ELIT limits both the m/z range and the peak capacity. For this reason, the FT-ELIT MS approach is most appropriate for wide m/z range applications whereas MR-TOF MS can provide advantages in a 'zoom-in' mode in which moderate resolution (M/ $\Delta M_{FWHM} \approx 10,000$ ) at short analysis times (10 ms) is desirable.

Keywords: Multi-reflectron time-of-flight, Fourier transform mass spectrometry, electrostatic linear ion trap

#### **INTRODUCTION**

Devices capable of trapping gaseous ions have become common-place in analytical mass spectrometry (MS) both as ion storage devices and as mass analyzers. Electrodynamic ion traps, such as the Paul trap<sup>1</sup> and linear quadrupole ion traps<sup>2,3</sup>, are commonly used as mass spectrometers and as devices for conducting multi-stage MS experiments (i.e., MS<sup>n</sup> where n>1). In most cases, mass analysis is conducted using a form of mass-selective instability<sup>4</sup> whereby ions are scanned out of the ion trap in an m/z-dependent fashion with external detection via an electron multiplier. The ion cyclotron resonance (ICR) ion trap, which combines trapping in the x- and y-dimensions using a strong magnetic field with electrostatic trapping in the z-dimension, can provide unparalleled mass resolution via Fourier transformation of time-domain signals generated by the detection of image currents on opposing electrodes to the frequency domain via Fourier transformation<sup>5,6</sup>. The ICR cell was the first to employ Fourier transform techniques for mass spectrometry and forms the basis for FT-ICR mass spectrometers<sup>7</sup>. A purely electrostatic ion trap based on orbital trapping<sup>8,9</sup>, referred to as the Orbitrap<sup>TM</sup>, was introduced by Makarov<sup>10,11</sup> that is also capable of FT-MS<sup>12</sup>. The generation of a differential time-domain image current on an outer electrode that is split into two halves facilitates Fourier-transformation to generate a mass spectrum. The Orbitrap<sup>TM</sup>, operated in the FT-MS mode, is also capable of generating very high mass resolution and is now widely used in applications that require high resolution and high mass measurement accuracy.

A conceptually very simple form of electrostatic ion trapping can be effected via the reflection of ions between two opposing ion mirrors, in analogy with an optical resonator. Such devices, referred to here as electrostatic linear ion traps (ELITs), have been used for mass analysis, although they are not as fully developed for mass spectrometry as the other forms of ion trapping devices mentioned above. A particularly prominent application of an ELIT is found in so-called charge detection mass spectrometry (CDMS) in which both the charge and the m/z ratio of a single ion are measured to determine ion mass. This application, first described by Benner<sup>13,14</sup>, and further developed by Jarrold et al. <sup>15,16,17</sup>, Dugourd et al. <sup>18,19</sup>, and Williams et al. <sup>20</sup>, relies on image charge measurements as individual large multiply charged ions pass through one or more central pick-up electrodes in the field-free region of an ELIT. The m/z ratio of the individual ion can be determined either via measurement of the time the ion takes to pass through a pick-up electrode<sup>21</sup> (i.e., an ion velocity measurement) or via Fourier transformation of the time-domain signal generated by the pick-up electrode (i.e., a frequency measurement). Zajfman et al. first described FT-ELIT MS on populations of ions, <sup>22,23</sup> in analogy with the FT-ICR and Orbitrap experiments.

A parallel line of work with ELITs has involved a time measurement in which ions undergo multiple reflections in an ELIT<sup>24,25</sup> followed by destructive detection typically using a microchannel plate detector. The latter work falls into the general category of closed-path multireflection time-of-flight mass spectrometry (MR-TOF MS), which has also been effected using electrostatic sectors<sup>26</sup> rather than ion mirrors. Several closed-path MR-TOF devices have been constructed for the purpose of high resolution mass selection and mass analysis for the study of short-lived nuclei<sup>27,28,29</sup> in radioactive beam facilities. However, a relatively compact MR-TOF designed for use as an analytical mass spectrometer has been described<sup>30</sup>.

We have been exploring the ELIT geometry as a component in a platform for MS<sup>n</sup> experiments for several reasons. These include, for example, the facility with which a device with a linear geometry can be coupled with other ion optical elements and the relative simplicity of a purely electrostatic ion trap. We have demonstrated, for example, non-destructive tandem mass spectrometry in a combined ELIT/quadrupole linear ion trap instrument whereby ions were passed back and forth between the ion traps without an intervening ionization step. Mass analysis of the precursor ions and the product ions were carried out via FT-ELIT MS whereas ion dissociation was conducted in the quadrupole ion trap<sup>31</sup>. We subsequently demonstrated ion isolation within the ELIT via modulation of one of the trapping electrodes<sup>32</sup> and surface-induced dissociation<sup>33</sup> at the end of the ELIT. The latter two developments enabled the execution of a tandem MS experiment using the ELIT for mass-selection, dissociation, and mass analysis of the products. In the course of this work, we have expended effort to optimize the FT-ELIT mass measurement in our apparatus<sup>34,35,36,37</sup>. However, a particularly attractive feature of the ELIT is that it is amenable to both FT-MS and closed-path MR-TOF MS measurements. Both forms of mass analysis can be performed simultaneously on the same population of ions as the two types of measurements are independent. In this work, we have adapted our current ELIT instrument for MR-TOF MS measurements while retaining the FT-MS capability. Each MS approach has its own relative strengths and weaknesses. While the MR-TOF measurement is as yet not fully optimized in this instrument, many of the key considerations in comparing time-based versus frequency-based measurements can be illustrated and point to the degree to which these approaches can be used to complement one another.

#### **EXPERIMENTAL SECTION**

**Materials.** Bromazepam, chlorprothixene HCl, gadolinium (III) chloride hexahydrate, and insulin (from bovine pancreas) were purchased from Sigma-Aldrich (St. Louis, MO, USA). Methanol (MeOH) was purchased from Thermo Fisher Scientific (Waltham, MA, USA). Glacial acetic acid (AcOH) was purchased from Mallinckrodt (Phillipsburg, NJ, USA). HPLC-grade water (H<sub>2</sub>O) was purchased from Fisher Scientific (Pittsburgh, PA, USA). The mixture of bromazepam (100 μM) and chlorprothixene HCl (5 μM) was prepared using 50/50 v/v MeOH/H<sub>2</sub>O. Insulin was prepared to a final concentration of 100 μM in 49.5/49.5/1 v/v/v MeOH/H<sub>2</sub>O/AcOH. Gadolinium(III) chloride hexahydrate was prepared to a concentration of 15 mM (49.5/49.5/1 v/v/v MeOH/H<sub>2</sub>O/AcOH).

**Mass Spectrometry.** All experiments were carried out on a home-built mass spectrometer depicted in Figure 1. A detailed description of the apparatus is provided in Supplemental Material. The nano-electrospray ionization (nESI) source and the method by which ions are concentrated and injected into the electrostatic linear ion trap (ELIT) have been described<sup>31,38</sup>. A brief description of the ion concentration and injection process is provided in Supplemental Information. Descriptions of the mass analysis approaches are provided below.

Fourier Transform Ion Detection and Signal Processing. The charge sensitive detection electronics have been described previously<sup>33,36</sup>. The preamplifier JFET was changed from a NTE452 to a BF862, resulting in a signal-to-noise enhancement factor of 1.9. The output of the charge sensitive preamplifier (A250, Amptek) was filtered (band-pass, Krohn-Hite Model 3940, Brockton, MA) and amplified (gain = 5) prior to digitization by a PCI-based digitizer (CS1621, 16-bit, Gage Applied Technologies, Lanchine, Quebec, Canada) at a rate of 10 MS/s (AC coupled, 1 MΩ input impedance, 25 MHz low-pass filter enabled). A program written in LabVIEW 13.0

(National Instruments, Austin, TX) was used to acquire each transient for FT analysis. A custom program, written in MATLAB 2015, was used to process the transients using the enhanced Fourier transform (eFT)<sup>39</sup>.

Multiple-Reflection Time-of-Flight. Dynamical time focus shifting (TFS)<sup>40</sup> was used on plates 8 and 1 (~2200 V) to shift the time focus of the ions to the center of the ELIT and the plane of the detector, respectively, thereby increasing the observed mass resolution. The TFS voltages were applied and pulsed using additional ORTEC 556 power supplies and solid-state switches (HTS 31-03-GSM). When ions were to be detected, plate 8 was pulsed from its nominal trapping potential to ground, allowing all ions to exit the ELIT and impinge upon a microchannel plate detector (MCP, APD 2 MINITOF 8/6/5/12 D 60:1 EDR SE, PS34049) manufactured by Photonis (Sturbridge, MA, USA). To detect positive ions, the input voltage lead was biased to -2200 V and the output voltage lead was connected to ground through a series 20 MΩ resistor to operate the SMA signal lead at ground. The signal was amplified by a Keithly Instruments (Cleveland, OH, USA) 108 wideband amplifier (50 Ω termination, 20 dB gain) prior to digitization by channel 2 of the CS1621 (50 Ω, 100 MS/s, DC coupled, 25 MHz low-pass filter enabled). All MR-TOF data were collected using the GaGeScope software provided with the digitizer and analyzed without further processing.

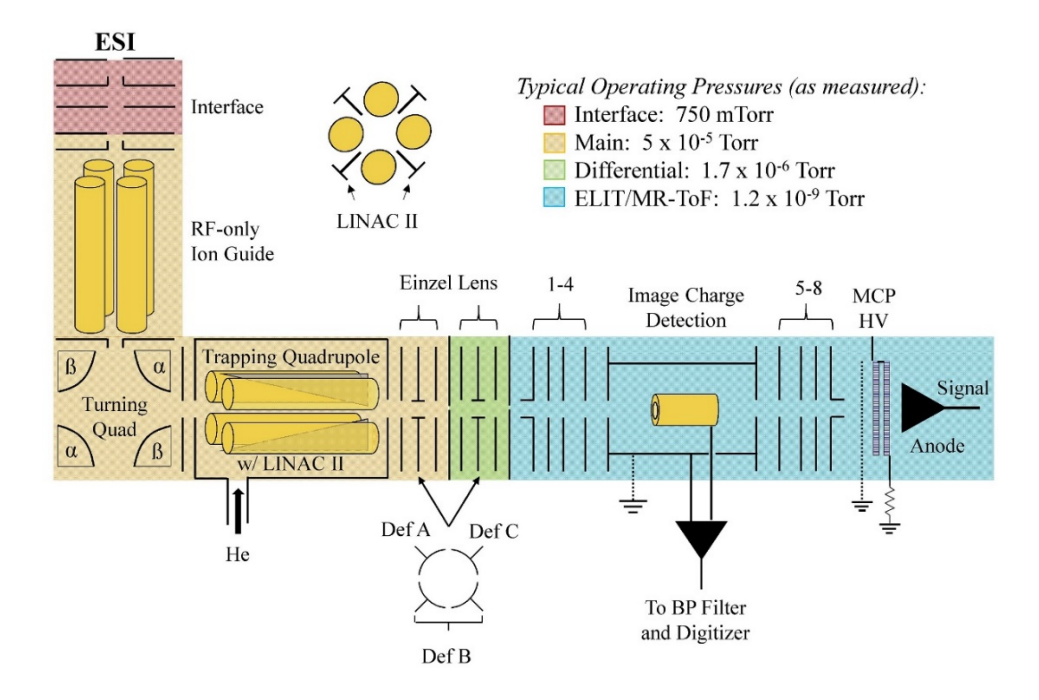


Figure 1 – Instrument schematic.

## RESULTS AND DISCUSSION

Each mass analysis approach is considered using a set of common mass analyzer figures of merit<sup>41</sup>. Results and/or commentary are provided here regarding mass resolution, mass measurement accuracy, *m/z* range, "peak capacity", and speed.

Mass resolution. Mass resolution, R, using the definition of  $R = M/\Delta M_{FWHM}^{42}$ , in an ELIT is given by  $f/2\Delta f$  in the FT-ELIT experiment and  $t/2\Delta t$  in the MR-TOF experiment, where f is ion frequency,  $\Delta f$  is the width of the peak at half height in the frequency domain signal, t is the ion flight time, and  $\Delta t$  is the width of the peak at half-height in the flight time spectrum. In the frequency measurement, in the absence of any ion loss or dephasing mechanisms, R increases linearly with acquisition time,  $T_{acq}$ , and decreases with the square root of the m/z of the ion according to:

$$R = CT_{acq}/(m/z)^{1/2}$$
 (1)

where C is a proportionality constant that depends on the apparatus. In practice, the useful  $T_{acq}$  is limited by the damping constant,  $\tau$ , which is the time for the time-domain signal to decay to  $1/e \approx 0.368$  of its original amplitude. The major contributor to the damping constant in our apparatus is collisions with background gas. The point is that R increases with measurement time until the signal is lost due to collisions/dephasing. (Based on a previously reported R = 36,900 at the fundamental frequency for ions at m/z 173.9 (i.e., the base peak of the GdO<sup>+</sup> isotopic envelope) at a  $T_{acq} = 300 \text{ ms}^{37}$ , C can be estimated to be  $1.622 \times 10^6$  for the present apparatus.) Figure 2 includes plots of R versus time for various scenarios. The dashed blue line represents R versus time up to 300 ms for an ion of m/z 316 under the FT-MS conditions used in our apparatus. We note that R has been observed to increase with the order of the detected harmonic, at least up to the third harmonic, in our apparatus<sup>37</sup>, which increases the slope of the resolution versus time relationship by a corresponding factor.

In the case of the MR-TOF experiment, R is approximately given by 43,27:

$$R = \frac{t_0/N + t_a}{2\sqrt{\left(\frac{\Delta t_0}{N}\right)^2 + (\Delta t_a)^2}} \tag{2}$$

where  $t_0$  is the flight time for a single pass from the ion injector to the detector, N is the number of passes through the ELIT,  $t_a$  is the flight time for a single lap in the ELIT,  $\Delta t_0$  is the initial time spread, which largely arises from the turn-around time associated with ion injection as well as any spatial spread in the injection quadrupole, and  $\Delta t_a$  is the additional time spread (i.e., dispersion) that occurs on each turn. The latter arises from imperfections in the performance of the mirrors, and/or trajectory variations. For our system,  $t_a$  is approximately given by:

$$t_a = 2(m/z)^{1/2}/K$$
 (3)

where m/z is the numerical value of the mass-to-charge ratio (unitless) and K = 3848700 Hz. Note that in the absence of  $\Delta t_a$ , R increases linearly with flight time with no limit. In any real device,  $\Delta t_a$  is non-zero such that, as  $N \to \infty$ :

$$R \to t_a/2\Delta t_a$$
 (4)

Figure 2 compares the dependence of resolution on storage time for an MR-TOF MS experiment (red data points), derived from relations (2) and (3), with that of an FT-ELIT MS experiment (blue data points), derived from relation (1), for an ion of m/z = 316 using values that apply, at least approximately, to the conditions used in these studies (viz.,  $t_0 = 10 \mu s$ ,  $\Delta t_0 = 110 ns$ ,  $\Delta t_a = 50 ps$ , K = 3858700,  $C = 1.622 \times 10^6$ ). In the case of the MR-TOF experiment, resolution approaches the maximum value of roughly 92,000 within about 100 ms under these conditions. It is clear from Figure 2 that R increases much more rapidly in the MR-TOF experiment relative to the FT-MS experiment during the first 50 ms of storage time. The figure indicates that a resolution slightly in excess of 20,000 can be achieved in 5 ms in the MR-TOF mode whereas an equivalent resolution

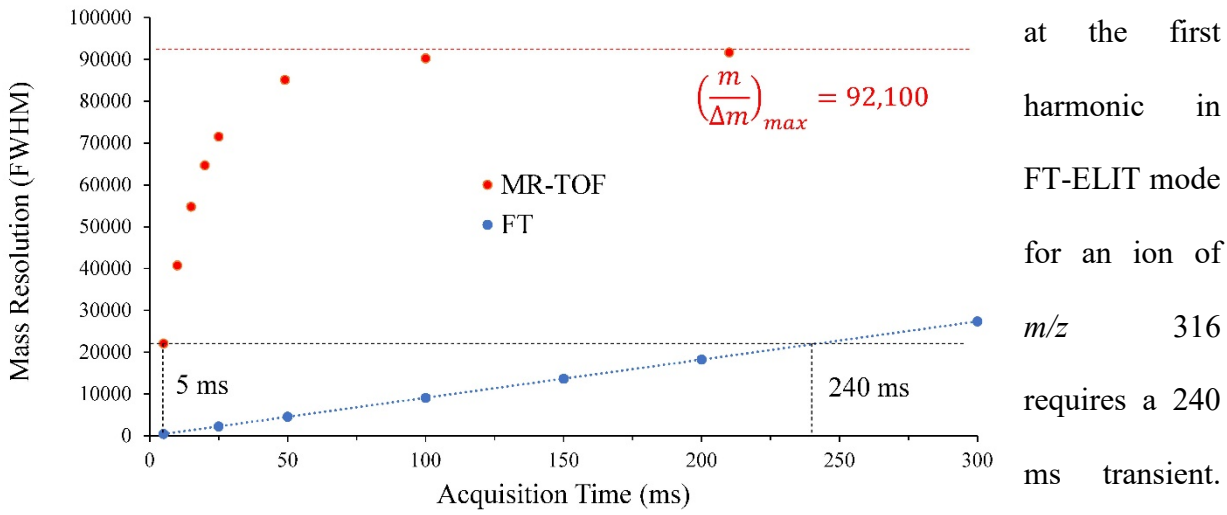


Figure 2 – Mass resolution versus acquisition (storage) time for the MR-TOF experiment (red data points) and the FT-ELIT experiment (blue data points) for an ion of m/z 316.

performance of the MR-TOF experiment is more sensitive to injection conditions than the FT-

ELIT experiment. The initial slope of the resolution versus time curve for the MR-TOF experiment is strongly dependent upon injection pulse width,  $\Delta t_0$  (see relation (2)). In the case of the FT-ELIT experiment, on the other hand, as long as an ion yields a time-varying signal at the pick-up electrode, the resolution of the FT-ELIT experiment is independent of pulse width.

Figure 3 compares insulin data acquired via nESI under various mass analysis conditions. Figure 3(a) shows the broad-band eFT-ELIT mass spectrum obtained over the first 75 ms of a 250 ms transient (100 averages, first harmonic). The data were restricted to the first 75 ms because the higher *m/z* ion signals decay relatively quickly. This spectrum shows an *m/z* range in excess of 5000. Figure 3(b) shows the eFT mass spectrum encompassing the isotopes of the 5+ charge state of bovine insulin derived from an 11.0913 ms transient (100 AVGS, 3<sup>rd</sup> harmonic). This spectrum shows no evidence for the individual isotopes. Figure 3(c) shows the eFT mass spectrum of the 5+ charge state of insulin derived from the full 250 ms transient (100 AVGS, 3<sup>rd</sup> harmonic), which results in a mass resolution of 32,000. Figure 3(d) shows the MR-TOF MS over the narrow *m/z* range of the 5+ insulin isotopes after a storage time of 11.0913 ms (1000 AVGS). This spectrum reflects a mass resolution of roughly 11,000 and should be compared directly with the spectrum of Figure 3(b). This comparison demonstrates experimentally that mass resolution increases more

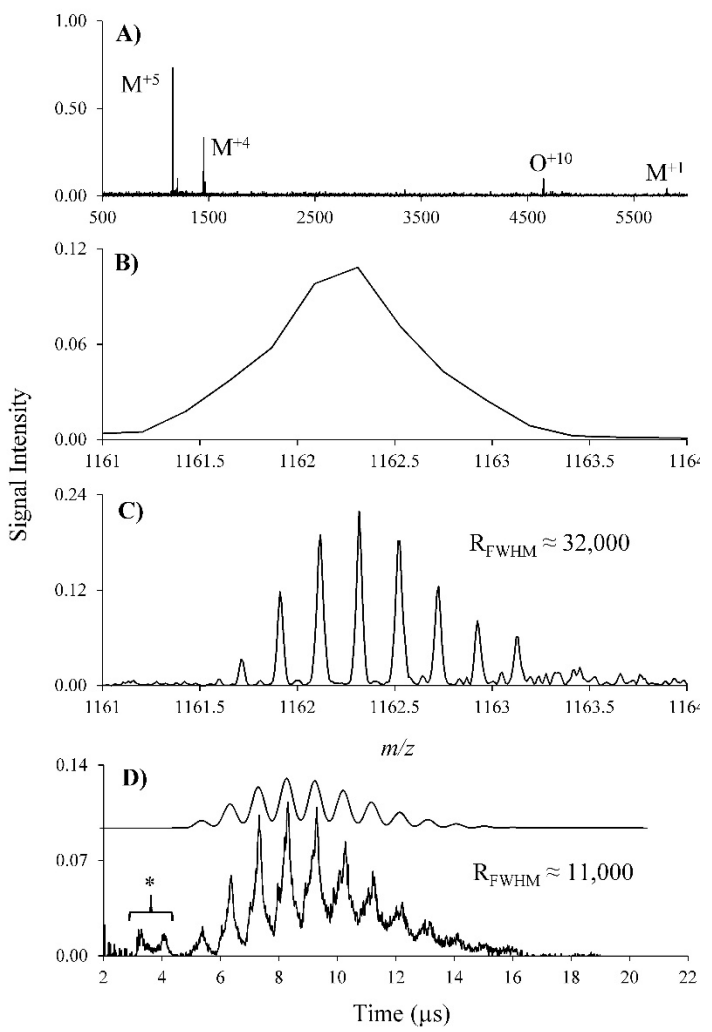


Figure 3: (A) eFT mass spectrum of insulin using a 250 ms transient (100 AVGS) that was truncated to 75 ms to observe the larger m/z ions. (B) eFT mass spectrum of insulin<sup>+5</sup> using a 11.0913 ms transient (100 AVGS, 3<sup>rd</sup> harmonic). (C) eFT mass spectrum of insulin<sup>+5</sup> using athe full 250 ms transient (100 AVGS, 3<sup>rd</sup> harmonic). (D) MR-TOF mass spectrum of insulin<sup>+5</sup> at 11.0913 ms (1000 AVGS). The theoretical isotopic distribution at a mass resolution of 11,000 is shown for comparison. The \* indicates peaks that arise from ions believed to be present in the region between plates 7 and 8 when plate 8 is pulsed down.

quickly with time in the MR-TOF measurement, at least at short times, than does the FT-ELIT measurement. note that a reviewer asked if the predicted maximum resolution is actually achieved at longer storage times. We believe so. However, it is not trivial to demonstrate. A major point of the paper is that the m/zrange decreases with the number of laps (see relation 6 and Figure 4 below). For the nominal m/z 316 ion used for the various figures, a storage time of 200 ms (>21,000 laps) that leads to a resolution of 92,000 results in an unlapped m/zrange of 20-30 milli-mass units. can't demonstrate such a resolution with the isobaric drugs used here because they differ in mass by a little over 80 millimass units.)

Mass measurement accuracy.

The main limitation to mass

measurement accuracy in our ELIT device is likely to arise from instabilities in the power supplies used to trap the ions. Such instabilities affect both the ion frequency and flight-time measurements.

Assuming both detection methods employ data acquisition rates sufficient to define the position of a peak, both approaches are ultimately limited by resolution and counting statistics according to the relationship:

$$\frac{\delta M}{M} = \frac{k}{R\sqrt{n}} \tag{5}$$

where  $\delta M$  is the difference between the measured mass and the true mass, k is a factor that has been reported to be approximately unity<sup>44</sup>, R is mass resolution as defined above, and n is the number of detected ions. This relationship has been used in the context of frequency measurements in a Penning trap<sup>41</sup> and time measurements made via MR-TOF<sup>45</sup>. Another report indicated a k value of  $1/(2(2 \ln 2)^{1/2})$  for the MR-TOF approach, assuming a Gaussian peak shape<sup>27</sup>. In any case, with careful calibration of the mass scale, both FT-MS and MR-TOF<sup>42,46</sup> approaches have demonstrated sub-ppm mass measurement accuracies. While we have not attempted to optimize mass measurement accuracy in the development of this instrument to date, we have observed mass measurement accuracies on the order of 10 ppm or less when using internal standards in our FT-ELIT measurements. Based on relation 5 and the results and discussion regarding mass resolution above, given the same number of ions per injection, mass measurement accuracy would be expected to improve faster with the MR-TOF measurement than with the FT-MS method such that high mass measurement accuracies would be expected to be achieved faster with MR-TOF. Indeed, the speed and accuracy of the MR-TOF measurement enabled the accurate mass measurement of short-lived calcium isotopes under conditions in which Penning trap measurements were too slow<sup>43</sup>. Alternatively, with the higher speed of the MR-TOF measurement, it should be possible to achieve better ion statistics than the FT-MS experiment at the same mass

resolution due to the greater number of measurement cycles that can be executed over a given time-scale.

M/z range. For all practical purposes, there is no upper or lower m/z limit for trapping and storing ions in an ELIT. There are constraints associated with detection methods for factors such as the minimum number of charges, in the case of image charge/current measurements, and the minimum ion velocity, in the case of electron multipliers. These factors can play a role in limiting the mass range but are not addressed here. The range of m/z values that can be studied for a given ion injection event into the ELIT for an FT-ELIT experiment has been discussed for both the intrap potential lift approach to ion capture<sup>36</sup> and for the mirror switching approach for ion capture<sup>35</sup>, as used here. Briefly, for mirror switching, the m/z range that can be captured is constrained by the flight time associated with a single reflection for the fastest ion of interest (i.e., the ion of lowest m/z ratio). The entrance gate must be closed before the fastest injected ion can reflect back and escape the ELIT via the entrance mirror. Any ion too slow (i.e., of m/z too high) to enter the ELIT during this gating window is prevented from entering the ELIT. For a given injection energy and set of trapping conditions, the m/z range of captured ions can be varied via the delay time between ion ejection from the accumulation quadrupole and the closing of the entrance mirror. For example, an m/z range of 500-5800 for a single set of ion injection conditions is demonstrated in Figure 3(a).

In the case of closed-path MR-TOF, the m/z range over which unambiguous mass assignments can be made is severely constrained by the so-called 'race track effect' whereby fast ions lap slower ions<sup>47</sup>. The ratio of highest m/z ion to the lowest m/z ion that can be stored without lapping in an ELIT as a function of the number of turns (laps), N, is approximately<sup>48</sup>:

$$\frac{m/z_{max}}{m/z_{min}} \approx \left(\frac{N+1}{N}\right)^2 \tag{6}$$

There is clearly a trade-off between resolution and m/z range for unambiguous mass assignment in the MR-TOF experiment. Figure 4 shows a plot of  $m/z_{\text{max}}/m/z_{\text{min}}$  versus lap number (blue line,

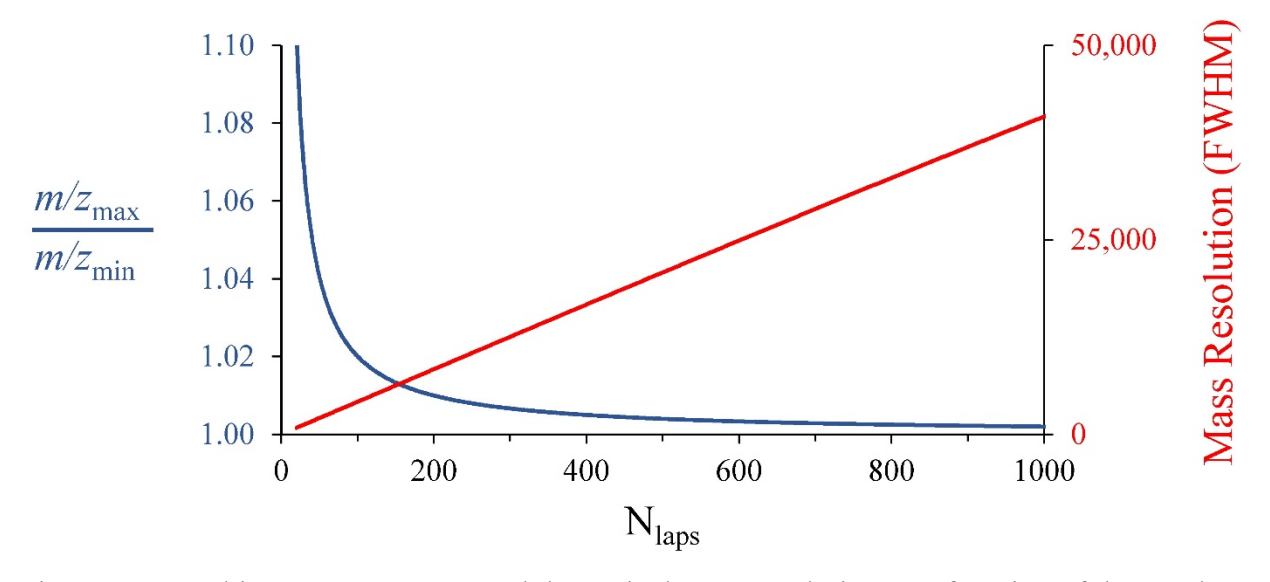


Figure 4: Unambiguous mass range and theoretical mass resolution as a function of the number of laps (N) for an ion of m/z 316. The parameters are as follows:  $t_0 = 10 \mu s$ ,  $\Delta t_0 = 110 ns$ , K = 3858700, and  $\Delta t_a = 50 ps$ .

left y-axis) and mass resolution for an ion of m/z 316, using the parameters given for Figure 2, versus lap number (right axis, red line). This plot clearly demonstrates how rapidly the unambiguous m/z range narrows with lap number. The potential for ambiguity in mass assignment at high resolution is usually minimized by injecting ions within a narrow distribution of m/z values and ejecting the trapped ions before lapping can take place for the mass-selected ion population.

A simple example illustrating the trade-off between resolution and m/z range is given in Figures 5(a) and 5(b), which compare MR-TOF data for a mixture of cations derived from the nESI of the drugs bromazepam ( $C_{14}H_{11}N_3OBr$ , monoisotopic m/z = 316.0085) and chlorprothixene ( $C_{18}H_{19}NSCl$ , monoisotopic m/z = 316.0921) at storage times of 1.1595 ms and 4.730 ms, respectively. For reference, the eFT mass spectrum obtained from a 150 ms transient is shown in

Figure 5(c). (The tailing in the MR-TOF data is believed to result from an asymmetric trapped ion kinetic energy distribution resulting from the non-linear extraction field of our injection method. This is not a fundamental characteristic of MR-TOF, as this would probably be eliminated if we were to use a push-pull technique for extracting the ions. We don't claim to have achieved a stateof-the-art approach to MR-TOF. However, it is certainly good enough to illustrate the relative strengths of MR-TOF versus FT-ELIT.) The monoisotopic drug ions are labelled as 1 and 2, while the single <sup>13</sup>C-containing ions are labelled 3 and 4, the <sup>81</sup>Br- and <sup>37</sup>Cl-containing ions are labelled 5 and 6, respectively, and the <sup>13</sup>C, <sup>81</sup>Br- and <sup>13</sup>C, <sup>37</sup>Cl-containing ions are labelled 7 and 8, respectively. In Figure 5(a), the signals for these ions are observed in the order expected for ions that undergo the same number of laps. In Figure 5(b), however, the pairs of ions (viz., 1 and 2, 3 and 4, 5 and 6, 7 and 8) are observed in the reverse order, while the correct order within each pair is preserved. The m/z range estimated for the 1.1595 ms storage time (126 laps) is 5 m/z units assuming  $m/z_{min} = 316$ . The m/z range for an ion of m/z = 316 stored for 4.73 ms (513 laps) is roughly 1 m/z unit. This is consistent with ions of each nominal m/z ratio (e.g., the two monoisotopic ions 1 and 2 at nominal m/z 316) undergoing the same number of laps but each successive pair of peaks undergoing one less cycle than the ions one unit lower in m/z (i.e., the ions at nominal m/z 317 undergo 512 laps). Hence, the pairs of ions within each m/z unit appear

in the correct order in Figure 5(b) but the ions of each successive nominal m/z ratio undergo one less lap than the ions of the preceding m/z ratio and are therefore detected in reverse order. While there are approaches that can mitigate the complications from fast ions lapping slow ions, such as mass selection prior to injection of ions into the trap, the race-track effect places a severe constraint on the use of a closed-path MR-TOF device for general usage as a mass spectrometer for a wide range of applications. The m/z window for unlapped ions can be moved over a very wide range

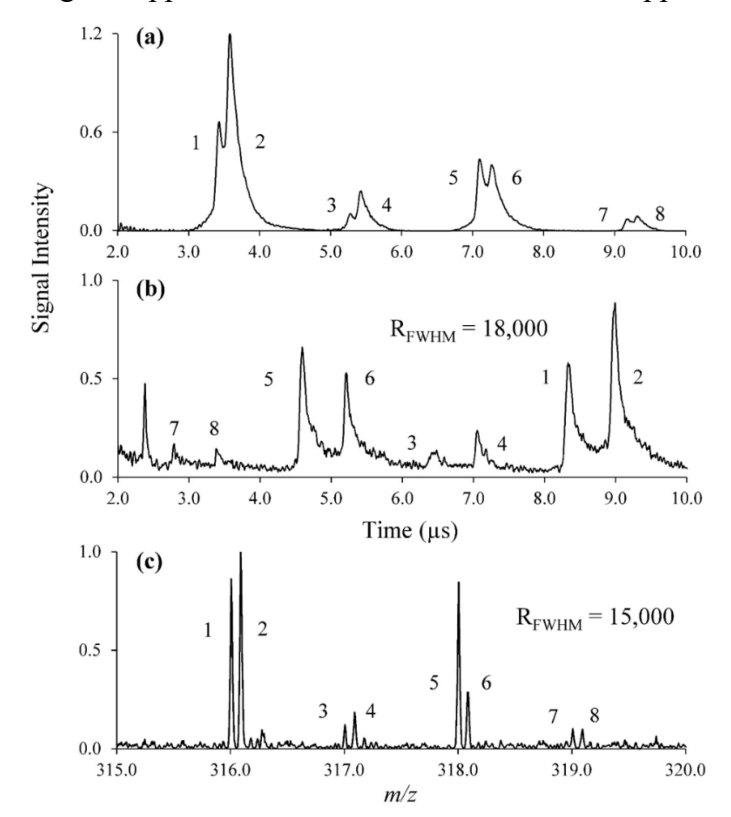


Figure 5: Mixture of bromazepam and chlorprothixene HCl cations detected at 1.1595 ms (a) and 4.730 ms (b) using MR-TOF. The eight isotopes are numerically labelled. (c) eFT mass spectrum of the same mixture at the fundamental frequency using a 150 ms transient (100 AVGS).

via an ion isolation step but it will be quite narrow at high resolution.

Peak capacity. The term "peak capacity" is usually encountered within the context of chromatography and refers to the number of peaks that can be resolved with a particular column<sup>49</sup>. It is an idealized figure of merit in that is assumes that the peaks are optimally distributed across the separation space. The actual number of peaks that are resolved in the non-ideal (i.e., "realworld") situation is usually much lower<sup>50</sup>. Within the context of mass

analysis, peak capacity is equal to the number of resolution elements (RE) across the accessible m/z range, which is given by<sup>51</sup>:

$$RE = \int_{m/z_{min}}^{m/z_{max}} \frac{R}{(m/z)} d(m/z)$$
 (7)

where R is the mass resolution defined above and  $m/z_{max}$  and  $m/z_{min}$  define the upper and lower limits to the m/z range. In the case where R is independent of m/z, such as the MR-TOF experiment<sup>30</sup>, the number of resolution elements is given by:

$$RE = Rln \frac{m/z_{max}}{m/z_{min}} \tag{8}$$

If the m/z range is restricted to nonlapped ions and N $\ge$ 1, relation (8) can be rewritten based on relations (2) and (6) as:

$$RE \approx \frac{\frac{t_0/N + t_a}{2\sqrt{\left(\frac{\Delta t_0}{N}\right)^2 + (\Delta t_a)^2}} ln\left(\frac{N+1}{N}\right)^2$$
 (9)

In the case where R is inversely related to  $(m/z)^{1/2}$ , which applies to the FT-ELIT experiment, the number of resolution elements is given by:

$$RE = CT_{acq} \left( \left( \frac{1}{\sqrt{m_{/z_{min}}}} \right) - \left( \frac{1}{\sqrt{m_{/z_{max}}}} \right) \right)$$
 (10)

where C and  $T_{acq}$  have been defined in relation (1). For any mass spectrometry experiment, peak capacity is determined by both the width of the resolution element(s) and the total width of the separation space (i.e., the m/z range). In the case of the FT-ELIT experiment, these two factors are independent of one another whereas they are inversely related in the closed cycle MR-TOF experiment. The result is that peak capacity increases linearly with resolution in the FT-MS experiment because the m/z range does not change. It is this characteristic of FT-ICR, for example, that makes it so well suited to applications like petroleomics<sup>52</sup>, which places a high premium on

peak capacity. An example of increasing peak capacity with storage (transient) time in the FT-ELIT experiment with the present instrument is given in Figure S-1 with mass spectra derived from the electrospray of a solution of GdCl<sub>3</sub> hexahydrate, which is dominated by GdO<sup>+</sup> ions and their adducts. All spectra were derived from different time segments (viz., (a) 4 ms, (b) 15 ms, (c) 75 ms, and (d) 300 ms) of the same 300 ms transient. The m/z range for this figure is arbitrarily restricted to m/z 150-m/z 500 due to the absence of ions at higher m/z ratios. The point is that the peak capacity, even at  $T_{acq} = 4$  ms, is already in excess of 200 and reaches nearly 18,000 at  $T_{acq} = 300$  ms within this m/z range.

The case is dramatically different in the closed-path MR-TOF experiment. Figure S-2 shows plots of RE versus N for an ion of m/z = 316 using approximate values for the current apparatus. Unlike the case with the FT-MS experiment, the number of resolution elements tends to decrease with storage time. Over the period in which the resolution continues to increase linearly with time, the number of resolution elements remains roughly constant. However, when the resolution begins to level off, the number of resolution elements decreases increasingly rapidly. The point at which this decrease becomes significant is largely determined by the dispersion term (i.e.,  $\Delta t_a$ ). The major point here is that the peak capacity of the MR-TOF measurement is relatively modest due to the rapidly decreasing m/z range with lap number (storage time) whereas it increases linearly with storage time in the FT-MS experiment. A commentary regarding peak capacity in closed-path MR-TOF when the non-lapped ion constraint is lifted is provided in Supplemental Information.

**Speed.** The foregoing results and discussion provide context for considering the relative analysis times for the MR-TOF and FT experiments in an ELIT. The MR-TOF approach can provide moderate resolution at significantly shorter analysis times than the FT approach but with

a limited *m/z* range. Furthermore, it is generally necessary to prevent ions from outside of the *m/z* range of interest from being injected into the ELIT in the MR-TOF experiment as such ions will appear in the mass spectrum at locations that are inconsistent with the mass calibration for the ions of interest. In order to generate data with the *m/z* range and peak capacity afforded by the FT experiment using MR-TOF, it is necessary to piece together a spectrum using multiple injections of isolated segments of the overall spectrum. In this scenario, the speed advantage of the MR-TOF is seriously compromised.

#### **CONCLUSIONS**

The linear electrostatic ion trap geometry allows for a straightforward combination of a frequency-based mass measurement (e.g., FT-ELIT MS) and a time-based measurement (e.g., MR-TOF MS). The FT-ELIT MS experiment affords a much larger m/z range, increasing peak capacity with time, and is less sensitive to initial injection pulse width. It can also provide superior mass resolution at long storage times, provided sufficiently long transients can be achieved. Mass resolution decreases with the inverse square root of ion m/z ratio with the FT experiment and tens to hundreds of charges are needed for image charge/current detection. With the MR-TOF experiment, mass resolution increases faster with storage time and is less strongly dependent upon m/z. Furthermore, in principle, it is possible to detect a single charge with a channel-plate detection scheme. However, the race-track effect associated with a closed-path MR-TOF experiment severely limits the m/z range for unambiguous mass measurement and also limits peak capacity. Taken collectively, the relative merits of these mass analysis approaches point to the use of the FT-ELIT MS scheme as most appropriate for broad m/z range mass analysis and the MR-TOF MS scheme as a complementary approach for 'zoom-in' targeted applications that can benefit from

faster measurements focused on a very narrow m/z range for the separation of isobaric ions, for example.

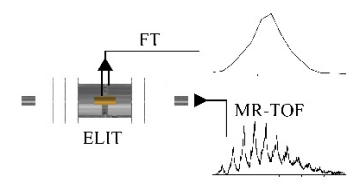
# **Supporting Information**

Additional text providing an instrument description, conditions used for ion injection, and a discussion of peak capacity in MR-TOF with the non-lapped constraint lifted; figures showing peak capacity increases with acquisition time in FT-ELIT MS and peak capacity as a function of lap number in MR-TOF MS.

## Acknowledgements

This work was supported by the Purdue Research Foundation and the National Science Foundation NSF CHE-1708338. The instrument was initially constructed with AB Sciex support. We thank Mark Carlsen, Randy Replogle, Phil Wyss, and Tim Selby of the Jonathan Amy Facility for Chemical Instrumentation for helpful discussions and their help with construction of the mass spectrometer. We also acknowledge Mircea Guna, and Dr. James W. Hager of AB Sciex for helpful discussions and for providing the collision cell with LINAC.

## For TOC only:



### References

(1) March, R.E.; Todd, J.F.J. (Eds.). *Quadrupole ion trap mass spectrometry*, second edition; John Wiley & Sons, Inc.: Hoboken, New Jersey, 2005

- (2) Schwartz, J.C.; Senko, M.W.; Syka, J.E.P. *J. Am. Soc. Mass Spectrom.* **2002**, *13*, 659-669.
- (3) Hager, J.W. Rapid Commun. Mass Spectrom. **2002**, 16, 512-526.
- (4) Stafford, G.C. Jr.; Kelly, P.E.; Syka, J.E.P.; Reynolds, W.E.; Todd, J.F.J.: *Int. J. Mass Spectrom. Ion Processes* **1984**, *60*, 85-98.
- (5) Marshall, A. G., Hendrickson, C. L., and Jackson, G. S. *Mass Spectrom. Rev.* **1998**, *17*, 1–35.
- (6) Marshall, A.G.; Hendrickson, C.L.; Shi, S. D.-H. *Anal. Chem.*, May 1, **2002**, 252A-259A.
- (7) Comisarow, M. B.; Marshall, A. G. Chem. Phys. Lett. 1974, 25, 282–283
- (8) Kingdon, K.H. Phys. Rev. 1923, 21, 408-418.
- (9) Knight, R.D. Appl. Phys. Lett. 1981, 38, 221-223.
- (10) Makarov, A. Anal. Chem. 2000, 72, 1156-1162.
- (11) Eliuk, S.; Makarov, A. Ann. Rev. Anal. Chem. 2015, 8, 61-80.
- (12) Scigelova, M.; Hornshaw, M.; Giannakopulos, Makarov, A. *Mol. Cell. Proteomics* **2011**, *10*, 1-19.
- (13) Benner, W.H. Anal. Chem. 1997, 69, 4162-4168.
- (14) Schultz, J. C., Hack, C. A., Benner, W. H. J. Am. Soc. Mass Spectrom. 1998, 9, 305-313.
- (15) Pierson, E.E., Keifer, D.Z., Contino, N.C., Jarrold, M.F. *Int. J. Mass Spectrom.* **2013**, *337*, 50-56.
- (16) Pierson, E. E., Contino, N. C., Keifer, D. Z., Jarrold, M. F. *J. Am. Soc. Mass Spectrom.* **2015**, *26*, 1213-1220.
- (17) Keifer, D. Z., Shinholt, D. L., Jarrold, M. F. Anal. Chem. 2015, 87, 10330-10337.
- (18) Doussineau, T., Kerleroux, M., Dagany, X., Clavier, C., Barbaire, M., Maurelli, J., Antoine, R., Dugourd, P. *Rapid Commun. Mass Spectrom.* **2011**, *25*, 617-623.
- (19) Doussineau, T.; Antoine, R.; Santacreu, M.; Dugourd, P. *J. Phys. Chem. Lett.* **2012**, *3*, 2141–2145.
- (20) Elliott, A.G.; Merenbloom, S.I.; Chakrabarty, S.; Williams, E.R. *Int. J. Mass Spectrom.* **2017**, *414*, 45-55.
- (21) Wuerker, R.F.; Shelton, H.; Langmuir, R. J. Appl. Phys. **1959**, 30, 342–349.
- (22) Ring, S.; Pedersen, H. B.; Heber, O.; Rappaport, M. L.; Witte, P.; Bhushan, K. G.; Altstein, N.; Rudich, Y.; Sagi, I.; Zajfman, D. *Anal. Chem.* **2000**, *72*, 4041-4046.
- (23) Zajfman, D.; Rudich, Y.; Sagi, I.; Strasser, D.; Savin, D.W.; Goldberg, S.; Rappaport, M.; Heber, O. *Int. J. Mass Spectrom.* **2003**, *229*, 55-60.
- (24) Wollnik, H.; Przewloka, M. Int. J. Mass Spectrom. Ion Processes 1990, 96, 267-274.
- (25) Wollnik, H.; Casares, A.; Radford, D.; Yavor, M., *Nucl. Instrum. Meth. A*, **2004**, *519*, 373-379.
- (26) Toyoda, M. Eur. J. Mass Spectrom. **2010**, 16, 397-406.
- (27) Plaß, W.R.; Dickel, T.; Scheidenberger, C. Int. J. Mass Spectrom. 2013, 349, 134-144.
- (28) Schury, P; Okada, K.; Shchepunov, S.; Sonoda, T.; Takamine, A.; Wada, M.; Wollnik, H.; Yamazaki, Y. *Eur. Phys. J. A* **2009**, *42*, 343-349.
- (29) Wolf, R.; Errit, M.; Marx, G.; Schweikhard, L. Hyperfine Interact. 2009, 199, 115-122.

- (30) Dickel, T.; Plaß, W.R.; Lang, J.; Ebert, J.; Geissel, H.; Haettner, E.; Jesch, C.; Lippert, W.; Petrick, M.; Scheidenberger, C.; Yavor, M.I. *Nucl. Instrum. Meth. B* **2013**, *317*, 779-784.
- (31) Hilger, R.T.; Santini, R.E.; McLuckey, S.A. Anal. Chem. 2013, 85, 5226-5232.
- (32) Hilger, R.T.; Santini, R.E.; McLuckey, S.A. Int. J. Mass Spectrom. 2014, 362, 1-8.
- (33) Hilger, R.T.; Santini, R.E.; McLuckey, S.A. Anal. Chem. 2014, 86, 8822-8828.
- (34) Hilger, R.T.; P.J. Wyss, P.J.; R.E. Santini, R.E.; McLuckey, S.A. *Anal. Chem.* **2013**, *85*, 8075-8079.
- (35) Dziekonski, E.T.; Santini, R.E.; McLuckey, S.A. Int. J. Mass Spectrom. 2016, 405, 1-8.
- (36) Dziekonski, E.T.; Johnson, J.T.; Hilger, R.T.; McIntyre, C.; Santini, R.E.; McLuckey, S.A. *Int. J. Mass Spectrom.* **2016**, *410C*, 12-21.
- (37) Dziekonski, E.T.; Johnson, J.T.; McLuckey, S.A. Anal. Chem. 2017, 89, 4392-4397.
- (38) Hilger, R.T., Dziekonski, E.T., Santini, R.E., McLuckey, S.A. *Int. J. Mass Spectrom.* **2015**, *378*, 281-287.
- (39) Lange, O., Damoc, E., Wieghaus, A., Makarov, A. *Int. J. Mass Spectrom.* **2014**, *369*, 16-22.
- (40) Dickel, T., Yavor, M.I., Lang, J., Plaß, W.R., Lippert, W., Geissel, H., Scheidenberger, C. *Int. J. Mass Spectrom.* **2017**, *412*, 1-7.
- (41) McLuckey, S.A.; J.M. Wells, J.M. Chem. Rev. 2001, 101, 571-606.
- (42) Murray, K.K.; Boyd, R.K.; Eberlin, M.N.; Langley, G.J.; Li, L.; Naito, Y. *Pure Appl. Chem.* **2013**, *85*, 1515-1609.
- (43) Wolf, R.N.; Wienholtz, F.; Atanasov, D.; Beck, D.; Blaum, K.; Borgmann, Ch.; Herfurth, F.; Kowalska, M.; Kreim, S.; Litvinov, Yu. A.; Lunney, D.; Manea, V.; Neidherr, D.; Rosenbusch, M.; Schweikhard, L.; Stanja, J.; Zuber, K. *Int. J. Mass Spectrom.* **2013**, *349-350*, 123-133.
- (44) Bollen, G. *Nuclear Physics A* **2001**, *693*, 3-18.
- (45) Schury, P.; Wada, M.; Ito, Y.; Naimi, S.; Sonoda, T.; Mita, H. Takamine, A.; Okada, K.; Wollnik, H.; Chon, S.; Haba, H.; Kaji, D.; Koura, H.; Miyatake, H.; Morimoto, K.; Morita, K.; Ozawa, A. *Nucl. Instrum. Meth B* **2013**, *317*, 537-543.
- (46) Wienholtz, F.; Beck, D.; Blaum, K.; Borgmann, Ch.; Breitenfeldt, M.; Cakirli, R.B.; George, S.; Herfurth, F.; J.D. Holt; Kowalska, M.; Kreim, S.; Lunney, D.; Manea, V.; Menéndez, J.; Neidherr, D.; Rosenbusch, M.; Schweikhard, L.; Schwenk, A.; Simonis, J.; Stanja, J.; Wolf, R.N.; Zuber, K. *Nature* **2013**, *498*, 346-349.
- (47) Schury, P.; Ito, Y.; Wada, M.; Wollnik, H. Int. J. Mass Spectrom. 2014, 359, 19-25.
- (48) Yavor, M.I.; Plaß, W.R.; Dickel, T.; Geissel, H.; Scheidenberger, C. *Int. J. Mass Spectrom.* **2015**, *381-382*, 1-9.
- (49) Giddings, J.C. Anal. Chem. 1967, 39, 1027-1028.
- (50) Davis, J.M.; Giddings, J.C. *Anal. Chem.* **1983**, *55*, 418-424.
- (51) Liu, J.; Chrisman, P.A.; Erickson, D.E.; McLuckey, S.A. *Anal. Chem.* **2007**, *79*, 1073-1081.
- (52) Marshall, A. G.; Rodgers, R. P. *Proc. Nat. Acad. Sci.*, **2008**, *105*, 18090–18095.